# Various collective states in the $^{124}$I nucleus

C.-B. Moon,* B. Moon, and J. Park
*Center for Exotic Nuclear Studies, The Institute for Basic Science (IBS), Daejeon 34126, Korea*

G. D. Dracoulis,† T. Kibédi, R. A. Bark,‡ A. P. Byrne, P. A. Davidson, G. J. Lane, and A. N. Wilson§
*Department of Nuclear Physics, Research School of Physics, The Australian National University, Canberra ACT2601, Australia*

(Received 3 November 2020; revised 14 February 2021; accepted 9 March 2021; published 22 March 2021)

The level structure of $^{124}$I ($Z = 53$, $N = 71$) has been studied via the $^{122}$Sn($^{7}$Li, $5n$) $^{124}$I reaction with a beam energy of 54 MeV. Through in-beam and out-of-beam $\gamma$-ray spectroscopy, the sophisticated low-lying levels including isomeric states and numerous collective states have been established for the first time. A positive-parity collective band built on the $10^{+}$ state at 1297 keV is interpreted as being associated with the combination of a proton and a neutron in the same intruder $h_{11/2}$ orbital, namely the $\pi h_{11/2} \nu h_{11/2}$ configuration. This band shows a typical quadrupole vibrational character. In contrast, the negative parity bands based on the $\pi g_{7/2} \nu h_{11/2}$ configuration show a soft triaxial rotation. An isomeric $8^{-}$ state at 689 keV with a half-life of 14 ns can be explained as a K isomer due to a proton with an $\Omega_p = 9/2$ in the $g_{9/2}$ orbital coupled to a neutron with an $\Omega_n = 7/2$ in the $h_{11/2}$ orbital. The excited states based on this $\pi g_{9/2} \nu h_{11/2}$ configuration show a coupled rotational structure. Another coupled rotational band built on the $6^{+}$ state at 714 keV is thought to be based on the $\pi g_{9/2} \nu d_{3/2}$ configuration.

DOI: 10.1103/PhysRevC.103.034318

## I. INTRODUCTION

Nuclei close to the magic numbers are suitable candidates for investigations of the nuclear shell structure as they contain a finite number of valence nucleons near a large shell gap, inducing nuclear deformation by breaking the spherical symmetry [1,2]. The tellurium nuclei (Te, $Z = 52$), with two protons outside the $Z = 50$ shell closure, are known as a representative vibrator with a small quadrupole deformation. In contrast, xenon (Xe, $Z = 54$) isotopes tend to feature a triaxial rotator with a $\gamma$-soft deformation showing $\gamma$-vibration excitations. As expected, the iodine nuclei, I with $Z = 53$ exhibit transitional structure between the vibrator of Te and the triaxial rotator of Xe [3,4]. For odd-mass I isotopes, low-lying states are dominated by proton particles in the $g_{7/2}$ and the $d_{5/2}$ orbitals above the $Z = 50$ shell gap. In addition, the intruder $h_{11/2}$ orbital with a high-angular momentum, $l = 5$, plays a distinctive role in inducing a variety of nuclear shapes. Indeed, the collective bands built on the proton ($\pi$) $h_{11/2}$ orbital in odd-mass I isotopes transform from a rotational structure to a vibrational structure with increasing neutron number. Figure 1 shows such a shape transition around $N = 68$ in which the $h_{11/2}$ collective structure follows the Xe core states at and below $N = 66$ while revealing the Te core vibrator at and above $N = 68$.

For Te and Xe nuclei with odd neutron numbers, dominant yrast states also are built on the neutron ($\nu$) $h_{11/2}$ orbital. Thus, it is expected that collective bands based on the configuration of the proton $h_{11/2}$ orbital coupled to the neutron $h_{11/2}$ orbital should appear in odd-odd I isotopes. Referring to Fig. 1, the band structure associated with $h_{11/2}$ orbital in $^{124}$I is expected to be a vibrator rather than a rotator. Furthermore, a proton hole in the $g_{9/2}$ orbital below $Z = 50$ contributes to developing a deformed rotational structure. The so-called $K$ isomers [6,7] require an axially deformed nuclear shape and tend to occur when high-$j$ orbitals, such as $h_{11/2}$ and $g_{9/2}$, are being filled in the upper part of the nuclear shell. Here the quantum number $K$ defines the projection of the total angular momentum onto the nuclear symmetry axis. For odd-odd I isotopes, the high-$K$ isomers are built upon a coupled configuration with the proton intruder $g_{9/2}$ and the neutron intruder $h_{11/2}$ orbitals. In this paper, for the odd-odd $^{124}$I, we present for the first time a detailed level scheme including the collective bands associated with the proton-particle $h_{11/2}$ orbital and the proton-hole $g_{9/2}$ orbital, respectively, coupled to the neutron $h_{11/2}$ orbital. Preliminary reports of the experiments were given in Refs. [8–10]. We note that a partial level scheme with negative parity was given in Ref. [11].

## II. EXPERIMENTAL PROCEDURES

The excited states of $^{124}$I were populated through the $^{122}$Sn($^{7}$Li, $5n$) reaction at a beam energy of 54 MeV. The beam was provided by the 14UD (Unit Doubled) tandem

*cbmoon@ibs.re.kr
†Deceased.
‡Present address: iThemba LABS, PO Box 722, Somerset West 71 29, South Africa.
§Present address: Faculty of Social Sciences, University of Stirling, Stirling FK9 4LA, UK.

 

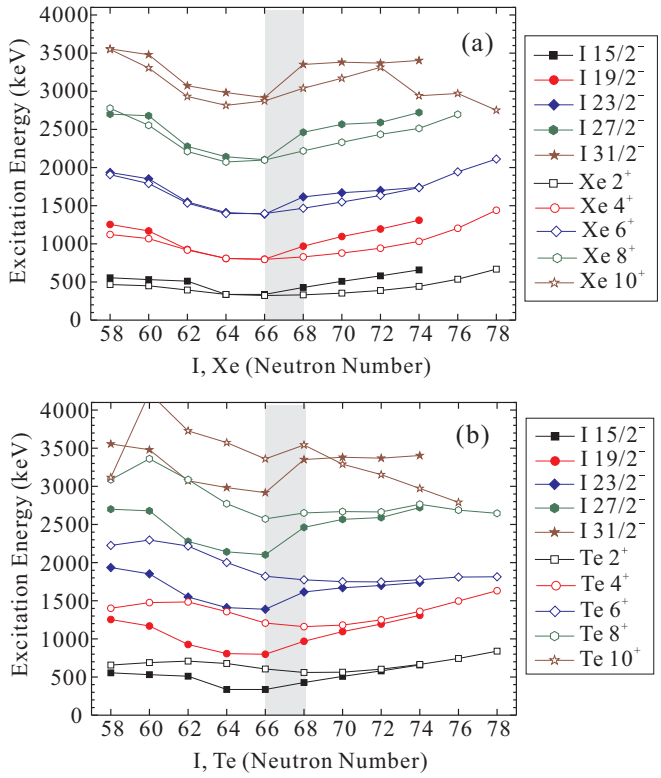


FIG. 1. Energy level systematic comparisons of the proton $h_{11/2}$ states of odd-mass I (filled symbols) with (a) the yrast states of even-mass Xe (open symbols) and with (b) the yrast states of even-mass Te (open symbols). The $11/2^-$ bandhead energies are set to be zero. The grey shadowed area represents a shape transition region. It should be noticed that the $10^+$ and $31/2^-$ states are dominated by the two-quasiparticle excitations in the $h_{11/2}$ orbital rather than the collective core excitations. Data are taken from the Evaluated Nuclear Structure Data at the National Nuclear Data Center [5].

accelerator at the Australian National University Heavy Ion Accelerator Facility (ANU-HIAF) [12]. Pulsed beams of 1 ns wide with a separation of 1.7 $\mu$s were used. The $^{122}$Sn target (enriched to 98.4%) was a self-supporting foil with a thickness of 3.5 mg/cm$^2$. $\gamma$ rays emitted during the decay of the excited states were detected using the CAESAR array, which consisted of 6 Compton-suppressed high-purity germanium (HPGe) detectors and two low-energy photon (LEP) detectors. The efficiency and energy calibrations were performed with $^{152}$Eu and $^{133}$Ba $\gamma$-ray sources. $\gamma$ rays were collected both during the period (*in-beam*) that the beam was incident on the target and during the *out-of-beam* period, allowing the detection of decays from isomeric states. Two sets of data were collected: (i) a singles measurement in which all $\gamma$ rays were timed relative to the beam pulse (beam-$\gamma$), and (ii) a $\gamma$-$\gamma$ coincidence measurement, also with timing relative to the beam pulse. The time difference between any two $\gamma$ rays in one event could then be reconstructed in subsequent analysis from the two time values relative to the beam pulse ($\gamma$-$\gamma$-$t$). The data were sorted into a series of two-dimensional matrices of 4096 by 4096 channels. The singles data were incremented into matrices with $\gamma$-ray energies on one axis and time on the other: one matrix containing data from the HPGe detectors, and another containing data from the LEP detectors. Several matrices were constructed from the coincidence data, taking either all combinations of HPGe detectors on both axes or any of the six HPGe detectors on one axis and either of the LEP detectors on the other. These matrices were created with various conditions on the time differences between the $\gamma$ rays, so that the data could be separated into groups of those $\gamma$ rays that were prompt, defined in this work as $\Delta T = \pm 140$ ns, with respect to each other and those that were separated in time (i.e., due to isomeric decays). A more detailed description regarding the present experiment including the coincidence relationships was given in Ref. [13]. Analysis of these data allowed a detailed determination of the level structure, especially the lifetimes of isomeric states and the precise location of transitions that precede or succeed them. $\gamma$-ray multipolarity information was extracted from the data using the method of directional correlation of oriented states (DCO ratios). The DCO ratios of the transitions, $R = I_\gamma(48^\circ \text{ or } 145^\circ)/I(97^\circ)$, were then determined wherever possible with sufficient statistics. In general, the ratios were determined by gating on stretched quadrupole transitions in the band sequence preceding or succeeding the transition of interest. Under the geometrical conditions of the detector, the total DCO projections indicate values close to 1.6 for stretched quadrupole transitions (mostly due to $E2$) and values close to 1.0 for stretched dipole transitions ($E1$ or $M1$). However, except for intense and isolated $\gamma$ rays, the total projection spectra did not yield concluding credit values due to contamination from other transitions. In contrast, the values based on the quadrupole (dipole) transition gates show close to 1.0 (1.6) for the quadrupole transitions and 0.6 (1.0) for dipole transitions. The spin-parity assignments for weak transitions, unfeasible from the DCO ratio analysis, were based on both the dipole-like $M1$ and quadrupole-like $E2$ transition relationships and the systematic trends of the level structure in a given collective band. The various DCO values as obtained by this approach are listed in Table I. Due to the presence of a few overlapping $\gamma$ rays originating from the competing channels, the transition intensities were derived from the coincidence spectra with gates on the $\gamma$ rays from the excited levels in $^{124}$I.

## III. EXPERIMENTAL RESULTS AND LEVEL SCHEME

Figure 2 shows the level scheme of $^{124}$I deduced from the present work. Except for some low-lying states obtained from the $(p,\gamma)$ reaction [14] and band 5 [11], the levels including several collective states were newly identified and their excitation energies were unambiguously established.

The ground state of $^{124}$I has spin and parity of $2^-$ with a half-life of $T_{1/2} = 4.18$ d [5]. Burde *et al.* [14] observed a $3^+$ isomer at an excitation energy of 55 keV, and measured its half-life to be $T_{1/2} = 52 \pm 5$ ns [hereafter denoted as 52(5) ns]. Our data confirmed this previous result but, as shown in Fig. 3, produce a little longer half-life at 63.5(7) ns. The errors include only statistical uncertainties. This value was obtained only from beam-$\gamma$ data due to an experimental limitation such as time walk experienced by low-energy $\gamma$ rays [13]. Thereby,

TABLE I. Excitation energies, $\gamma$-ray energies, relative intensities, DCO ratios, and spin-parity assignments to $^{124}$I. The half-lives of the isomeric states are given as well. The numbers in parentheses are the errors in the last digit.

A. Low-lying states. The half-lives of the isomeric states are given in the last column and the quoted uncertainties are statistical only.

| $E_i$ (keV) | $E_f$ (keV) | $E_\gamma$ (keV) | $I_\gamma$[a] | DCO[c] | Multipolarity | $J_i^\pi \rightarrow J_f^\pi$ | Half-life (ns) |
|---|---|---|---|---|---|---|---|
| 55.2 | 0.0 | 55.2(3) | 24(7) | | $E1$ | $3^+ \rightarrow (2^-)$ | 63.5(7) |
| 162.8 | 55.2 | 107.6(2) | 39(6) | 0.91(7)[i] | dipole | $\rightarrow 3^+$ | |
| 250.1 | 162.8 | 87.0(3) | 25(6) | 0.98(13)[i] | dipole | $(4^+) \rightarrow$ | 13.4(8) |
| | 55.2 | 194.6(4) | 23(5) | 0.93(17)[i] | dipole | $(4^+) \rightarrow 3^+$ | |
| 426.3 | 250.1 | 176.2(2) | 40(4) | 1.05(15)[g] | dipole | $(5^+) \rightarrow (4^+)$ | |
| 122.8 | 0 | 122.8(2) | 1000 | 1.11(3)[d], 1.02(4)[e], 1.75(3)[g] | $E2$ | $4^- \rightarrow 2^-$ | 10.6(3) |
| 286.8 | 122.8 | 164.0(2) | 807(10) | 1.10(3)[d], 1.03(2)[e], 1.83(3)[g] | $E2$ | $6^- \rightarrow 4^-$ | |
| 274.8 | 122.8 | 152.0(2) | 585(11) | 0.71(5)[d], 0.70(3)[e], 1.22(5)[g] | $M1/E2$ | $5^- \rightarrow 4^-$ | |
| 286.8 | 274.8 | 12.0(10)[b] | | | | | |
| 310.8 | 286.8 | 24.0(10)[b] | | | | $7^- \rightarrow 6^-$ | |
| 453.4 | 310.8 | 142.6(2) | 865(10) | 0.56(2)[d], 0.53(2)[e], 0.85(5)[g] | $M1/E2$ | $8^- \rightarrow 7^-$ | |
| 466.4 | 274.8 | 191.6(5) | | 0.54(22)[e] | $M1/E2$ | $6^- \rightarrow 5^-$ | |
| 535.9 | 466.4 | 69.5(9) | | | | | |
| | 287.8 | 248.1(6) | | | | | |
| 556.5 | 310.8 | 245.7(2) | 349(10) | 0.56(4)[d], 0.51(3)[e] | $M1/E2$ | $8^- \rightarrow 7^-$ | |
| 558.9 | 286.8 | 272.2(3) | | 0.74(16)[d] | $M1/E2$ | $7^- \rightarrow 6^-$ | |
| | 453.4 | 105.3(6) | | | $M1/E2$ | $7^- \rightarrow 8^-$ | |
| 689.3 | 558.7 | 130.4 | | 0.83(12)[e], 0.83(15)[h] | $M1/E2$ | $8^- \rightarrow 7^-$ | 13.7(4) |
| | 453.4 | 235.7(2) | 91(5) | 0.78(25)[d], 0.94(18)[e] | $M1/E2$ | $8^- \rightarrow 8^-$ | |
| | 310.8 | 378.9(5) | | | $M1/E2$ | $8^- \rightarrow 7^-$ | |
| | 556.5 | 132.6(4) | 42(7) | 1.03(22)[e], 1.33(7)[g] | $M1/E2$ | $8^- \rightarrow 8^-$ | |
| 755.4 | 453.4 | 301.9(2) | 523(12) | 0.54(4)[d], 0.42(3)[e] | $M1/E2$ | $9^- \rightarrow 8^-$ | |
| | 556.5 | 198.9(3) | 150(11) | 0.51(31)[d], 0.55(17)[e] | $M1/E2$ | $9^- \rightarrow 8^-$ | |
| 880.0 | 535.0 | 345.0(5) | | 0.36(17)[e] | $M1/E2$ | $8^- \rightarrow$ | |
| 935.7 | 453.4 | 482.0(4) | 122(10) | 0.51(33)[d], 0.86(25)[e] | $M1/E2$ | $8^- \rightarrow 8^-$ | |
| | 310.8 | 625.1(5) | 74(8) | 0.79(28)[d], 0.63(20)[e] | $M1/E2$ | $8^- \rightarrow 7^-$ | |
| | 286.8 | 649.0(3) | 88(7) | 1.74(35)[e] | $E2$ | $8^- \rightarrow 6^-$ | |
| 1078.3 | 556.5 | 521.6(6) | | 0.64(38)[e] | $M1/E2$ | $9^- \rightarrow 8^-$ | |
| | 310.8 | 767.7(3) | 78(6) | 1.03(41)[d], 0.98(24)[e] | $E2$ | $9^- \rightarrow 7^-$ | |
| 1244.9 | 755.4 | 489.4(1) | 260(35) | 1.03(7)[d], 1.11(8)[e] | $E2$ | $9^- \rightarrow 9^-$ | |
| | 556.5 | 689.1(8) | | | | $9^- \rightarrow 8^-$ | |
| | 453.4 | 791.3(2) | 217(10) | 0.564(4)[d], 0.54(2)[e] | $M1/E2$ | $9^- \rightarrow 8^-$ | |
| | 935.7 | 308.9(2) | 120(11) | 0.55(18)[d], 0.53(12)[e] | $M1/E2$ | $9^- \rightarrow 8^-$ | |
| | 880.0 | 364.8(3) | | 0.62(23)[e] | $M1/E2$ | $9^- \rightarrow 8^-$ | |
| 1296.5 | 1244.9 | 51.6(3) | | 0.55(45)[d], 0.46(27)[e] | $E1$ | $10^+ \rightarrow 9^-$ | |
| | 1078.3 | 218.0(3) | 42(8) | 0.61(28)[d], 0.57(16)[e] | $E1$ | $10^+ \rightarrow 9^-$ | |
| | 755.4 | 541.0(5) | 63(7) | 0.61(15)[d], 0.67(11)[e] | $E1$ | $10^+ \rightarrow 9^-$ | |

B. Band 1 built on the $10^+$ state at 1296.5 keV. The $I_\gamma$ values (column 4) are normalized to 100 for the 689.1-keV transition when gating on the 123-keV transition.

| $E_i$ (keV) | $E_f$ (keV) | $E_\gamma$ (keV) | $I_\gamma$ | $I_\gamma$[a] | DCO[b] | Multipolarity | $J_i^\pi \rightarrow J_f^\pi$ |
|---|---|---|---|---|---|---|---|
| 1681.4 | 1296.5 | 384.9(2) | 22(3) | 156(10) | 0.78(17)[d], 0.44(14)[e] | $M1/E2$ | $11^+ \rightarrow 10^+$ |
| 1985.6 | 1296.5 | 689.1(2) | 100 | 605(11) | 1.00(2)[d], 0.94(3)[e] | $E2$ | $12^+ \rightarrow 10^+$ |
| | 1681.4 | 304.2(3) | 7(1) | 56(7) | 1.02(21)[e] | $M1/E2$ | $4^+ \rightarrow 11^+$ |
| 2343.5 | 1681.4 | 661.8(4) | 12(1) | 69(6) | 0.98(3)[f] | $E2$ | $13^+ \rightarrow 11^+$ |
| | 1985.6 | 357.7(5) | 49(3) | 385(11) | 0.53(3)[d], 0.62(7)[e] | $M1/E2$ | $14^+ \rightarrow 13^+$ |
| 2682.0 | 1985.6 | 696.3(2) | 47(2) | 359(12) | 1.13(4)[d], 0.96(4)[e] | $E2$ | $14^+ \rightarrow 12^+$ |
| | 2343.3 | 338.7(3) | 15(2) | 147(10) | 0.57(14)[d], 0.42(11)[e] | $M1/E2$ | $14^+ \rightarrow 13^+$ |
| 2907.7 | 2343.3 | 564.5(7) | 22(1) | 177(11) | 0.86(9)[d], 0.95(9)[f] | $E2$ | $15^+ \rightarrow 13^+$ |
| | 2682.0 | 225.5(2) | 37(2) | 275(13) | 0.54(6)[d]. 0.50(7)[e] | $M1/E2$ | $15^+ \rightarrow 14^+$ |
| 3205.6 | 2682.0 | 523.4(8) | 5(1) | 24(7) | 1.16(38)[d] | $E2$ | $16^+ \rightarrow 14^+$ |
| | 2907.7 | 298.1(2) | 41(3) | 390(12) | 0.62(4)[d], 0.57(3)[f] | $M1/E2$ | $15^+ \rightarrow 14^+$ |
| 3887.8 | 2907.7 | 981.1(10) | 1.0(4) | | 1.62(46)[g] | $E2$ | $17^+ \rightarrow 15^+$ |
| | 3205.6 | 681.2(7) | 8(2) | 191(9) | 0.47(21)[d], 0.88(12)[g] | $M1/E2$ | $17^+ \rightarrow 16^+$ |

TABLE I. (*Continued.*)

| $E_i$ (keV) | $E_f$ (keV) | $E_\gamma$ (keV) | $I_\gamma$ | $I_\gamma$[a] | DCO[b] | Multipolarity | $J_i^\pi \rightarrow J_f^\pi$ |
|---|---|---|---|---|---|---|---|
| 4364.8 | 3205.6 | 1159.9(5) | 9(2) | 84(8) | 1.03(26)[d] | $E2$ | $18^+ \rightarrow 16^+$ |
| | 3887.8 | 478.3(12) | 1.0(5) | | | $M1/E2$ | $18^+ \rightarrow 17^+$ |
| 4966.8 | 3887.8 | 1079.3(3) | 3(1) | 21(5) | 1.69(11)[g] | $E2$ | $19^+ \rightarrow 17^+$ |
| | 4364.8 | 601.6(5) | 8(1) | 10(5) | 0.83(23)[g] | $M1/E2$ | $19^+ \rightarrow 18^+$ |
| 5341.4 | 4364.8 | 976.3(6) | 1.0(5) | | 1.79(51)[g] | $E2$ | $20^+ \rightarrow 18^+$ |
| | 4966.8 | 374.9(3) | 2(1) | | 1.08(48)[g] | $M1/E2$ | $20^+ \rightarrow 19^+$ |
| 4093.6 | 3205.6 | 887.9(2) | 4(1) | 49(6) | 0.36(37)[d], 0.81(33)[g] | $M1/E2$ | $17^+ \rightarrow 16^+$ |
| | 2907.7 | 1185.9(5) | 1.0(5) | 8(2) | 1.75(48)[g] | $E2$ | $17^+ \rightarrow 15^+$ |
| 4365.8 | 4093.6 | 272.2(3) | 9(2) | | 0.51(18)[e], 0.89(11)[g] | $M1/E2$ | $18^+ \rightarrow 17^+$ |
| 5515.4 | 4365.8 | 1149.6(3) | 1.0(5) | 15(3) | 1.65(33)[g] | $E2$ | $20^+ \rightarrow 18^+$ |

C. Bands 2 to 5

| $E_i$ (keV) | $E_f$ (keV) | $E_\gamma$ (keV) | $I_\gamma$[a] | DCO[c] | Multipolarity | $J_i^\pi \rightarrow J_f^\pi$ |
|---|---|---|---|---|---|---|
| Bands 2, 3 | | | | | | |
| 1134.5 | 453.4 | 681.2(3) | 191(11) | 0.97(3)[e] | $E2$ | $10^- \rightarrow 8^-$ |
| 1893.1 | 1134.5 | 758.6(2) | 172(9) | 1.14(4)[e] | $E2$ | $12^- \rightarrow 10^-$ |
| 2746.3 | 1893.1 | 852.8(2) | 115(9) | 0.99(12)[e] | $E2$ | $14^- \rightarrow 12^-$ |
| 3745.3 | 2746.3 | 999.0(2) | 46(8) | 1.09(32)[e], 1.08(25)[f] | $E2$ | $16^- \rightarrow 14^-$ |
| 4652.3 | 3745.3 | 907.0(3) | 29(5) | 0.98(28)[e] | $E2$ | $18^- \rightarrow 16^-$ |
| 1490.0 | 755.4 | 734.5(3) | 174(11) | 1.10(5)[e] | $E2$ | $11^- \rightarrow 9^-$ |
| 2358.9 | 1490.0 | 868.9(2) | 149(10) | 0.90(8)[e] | $E2$ | $13^- \rightarrow 11^-$ |
| 3382.4 | 2358.9 | 1023.5(2) | 45(8) | 1.22(25)[e]. 1.17(11)[f] | $E2$ | $15^- \rightarrow 13^-$ |
| 4395.2 | 3382.4 | 1012.8(6) | 31(6) | | | |
| 1134.5 | 755.4 | 379.0(2) | 176(10) | 0.46(6)[e] | $M1/E2$ | $10^- \rightarrow 9^-$ |
| 1490.0 | 1134.5 | 355.4(3) | 65(6) | | $M1/E2$ | $11^- \rightarrow 10^-$ |
| 1893.1 | 1490.0 | 403.0(4) | 87(7) | 0.28(15)[e] | $M1/E2$ | $12^- \rightarrow 11^-$ |
| 2746.3 | 2358.9 | 387.7(8) | | | $M1/E2$ | $14^- \rightarrow 13^-$ |
| 3860.1 | 2746.3 | 1113.8(3) | 19(5) | | | |
| | 3382.4 | 477.7(8) | | | | |
| Bands 4, 5 | | | | | | |
| 1303.6 | 556.5 | 747.1(3) | 78(7) | 1.19(8)[e] | $E2$ | $10^- \rightarrow 8^-$ |
| 2115.9 | 1303.6 | 812.1(3) | 37(5) | 1.01(11)[e] | $E2$ | $12^- \rightarrow 10^-$ |
| 3099.4 | 2116.1 | 983.5(3) | 20(6) | 1.16(33)[f] | $E2$ | $14^- \rightarrow 12^-$ |
| 2115.9 | 1304.5 | 811.6(6) | 15(4) | | | $12^- \rightarrow 10^-$ |
| 2762.1 | 2115.9 | 646.2(3) | 36(6) | 0.68(14)[e] | $M1/E2$ | $13^- \rightarrow 12^-$ |
| 2735.3 | 2115.9 | 619.4(5) | | 0.21(18)[e] | $M1/E2$ | $13^- \rightarrow 12^-$ |
| | 1893.1 | 842.2(3) | 16(5) | 0.24(17)[e], 0.30(11)[f] | $M1/E2$ | $13^- \rightarrow 12^-$ |
| 2762.1 | 1893.1 | 868.9(5) | 15(5) | 0.68(11)[f] | $M1/E2$ | $13^- \rightarrow 12^-$ |
| 2788.7 | 1893.1 | 895.6(4) | 12(4) | 0.63(23)[e], 0.68(22)[f] | $M1/E2$ | $13^- \rightarrow 12^-$ |
| 3484.4 | 2788.7 | 696.3(3) | 17(5) | 0.85(15)[f] | $E2$ | $15^- \rightarrow 13^-$ |
| | 2735.3 | 748.8(7) | 53(7) | 1.19(16)[e], 0.90(12)[f] | $E2$ | $15^- \rightarrow 13^-$ |
| | 2762.1 | 721.5(4) | 55(8) | 1.16(18)[e], 1.10(13)[f] | $E2$ | $15^- \rightarrow 13^-$ |
| | 2569.5 | 915.2(5) | 8(2) | 2.10(41)[h] | $E2$ | $15^- \rightarrow 13^-$ |
| 4210.8 | 3484.4 | 726.4(2) | 105(11) | 1.09(11)[e] | $E2$ | $17^- \rightarrow 15^-$ |
| 4863.1 | 4210.8 | 652.3(3) | 100(8) | 0.78(15)[e], 1.04(9)[f] | $E2$ | $19^- \rightarrow 17^-$ |
| 5555.2 | 4863.2 | 691.7(3) | 44(6) | 0.85(18)[f] | $E2$ | $21^- \rightarrow 19^-$ |

D. Band 6.

| $E_i$ (keV) | $E_f$ (keV) | $E_\gamma$ (keV) | $I_\gamma$[a] | DCO[c] | Multipolarity | $J_i^\pi \rightarrow J_f^\pi$ |
|---|---|---|---|---|---|---|
| 946.8 | 689.3 | 257.5(2) | 143(11) | 0.84(5) [e], 1.31(6)[g] | M1/E2 | $9^- \rightarrow 8^-$ |
| 1304.7 | 946.8 | 357.7(2) | 120(10) | 0.62(7) [e],1.06(5)[g],0.97(3)[h] | M1/E2 | $10^- \rightarrow 9^-$ |
| 1705.3 | 1304.7 | 400.6(5) | 52(7) | 1.03(3)[h] | M1/E2 | $11^- \rightarrow 10^-$ |
| 2129.9 | 1705.3 | 424.1(3) | 41(7) | 0.99(4)[h] | M1/E2 | $12^- \rightarrow 11^-$ |
| 2569.5 | 2129.9 | 439.6(5) | 30(6) | 1.14(8)[g] | M1/E2 | $13^- \rightarrow 12^-$ |
| 3022.8 | 2569.5 | 453.2(6) | 8(3) | 1.21(14)[g] | M1E2 | $14^- \rightarrow 13^-$ |
| 1304.7 | 689.3 | 615.6(3) | 62(5) | 1.51(34)[g] | E2 | $10^- \rightarrow 8^-$ |

TABLE I. (*Continued.*)

| $E_i$ (keV) | $E_f$ (keV) | $E_\gamma$ (keV) | $I_\gamma$[a] | DCO[c] | Multipolarity | $J_i^\pi \rightarrow J_f^\pi$ | Half-life (ns) |
|---|---|---|---|---|---|---|---|
| 2129.9 | 1304.7 | 825.6(4) | 32(7) | 1.37(21)[h] | E2 | $12^- \rightarrow 10^-$ | |
| 3022.8 | 2129.9 | 892.3(6) | 29(5) | 1.26(36)[h] | E2 | $14^- \rightarrow 12^-$ | |
| 1705.3 | 946.8 | 758.6(3) | 45(5) | 1.00(5)[e], 1.57(23)[g] | E2 | $11^- \rightarrow 9^-$ | |
| 2569.5 | 1705.3 | 864.2(3) | 34(5) | 1.20(21)[e] | E2 | $13^- \rightarrow 11^-$ | |

E. Bands 7, 8, 9. The $\gamma$-ray intensities ($I_\gamma$) are normalized to 100 for the 298-keV transition. Notice that bands 7, 8, and 9 are about 4% in intensity relative to the 123-keV transition.

| $E_i$ (keV) | $E_f$ (keV) | $E_\gamma$ (keV) | $I_\gamma$ | DCO[c] | Multipolarity | $J_i^\pi \rightarrow J_f^\pi$ |
|---|---|---|---|---|---|---|
| 714.7 | 426.3 | 288.4(3) | 54(4) | 0.95(4)[i] | $M1/E2$ | $(6^+) \rightarrow (5^+)$ |
| 1066.4 | 714.7 | 351.9(5) | 34(3) | 1.65(5)[i] | $M1/E2$ | $(7^+) \rightarrow (6^+)$ |
| 1457.7 | 1066.4 | 391.5(7) | 14(2) | 1.70(7)[i] | $M1/E2$ | $(8^+) \rightarrow (7^+)$ |
| | 714.7 | 743.3(3) | 6(2) | | | $(8^+) \rightarrow (6^+)$ |
| 1872.2 | 1457.7 | 414.6(8) | 7(2) | | | $\rightarrow (8^+)$ |
| | 1066.4 | 805.6(5) | 5(3) | | | $\rightarrow (7^+)$ |
| 724.4 | 426.3 | 298.1(3) | 100 | 0.74(3)[i] | $M1$ | $(6^+) \rightarrow (5^-)$ |
| 1080.6 | 426.3 | 654.3(3) | 53(3) | 2.27(8)[i] | $E2$ | $(7^+) \rightarrow (5^+)$ |
| 1432.1 | 724.4 | 707.7(3) | 51(3) | 2.19(12)[i] | $E2$ | $(8^+) \rightarrow (6^+)$ |
| 1809.6 | 1080.3 | 729.4(3) | 42(4) | 2.35(15)[i] | $E2$ | $(9^+) \rightarrow (7^+)$ |
| 2171.5 | 1432.1 | 739.4(3) | 18(4) | 2.31(17)[i] | $E2$ | $(10^+) \rightarrow (8^+)$ |
| 2561.4 | 1809.6 | 751.8(8) | 27(4) | 2.41(20)[i] | $E2$ | $(11^+) \rightarrow (9^+)$ |
| 3195.7 | 2561.4 | 634.3(4) | 15(4) | | | $\rightarrow (11^+)$ |

[a]The values are normalized to 1000 for the 123-keV transition.
[b]Derived from the level energy differences.
[c]DCO ratios are based on the gate spectrum setting on the following transitions.
[d]689–696 keV transitions (stretched quadrupole type) sum gate.
[e]123 and 164 keV transitions sum gate.
[f]A stretched quadrupole transition type gate such as 689, 734, 747, 726 keV, etc.
[g]A stretched dipole type transition gate such as 246, 302, 258 keV, etc.
[h]258-keV transition gate for band 6.
[i]176-keV transition gate for bands 7, 8, and 9.

a longer time may be caused by any delayed transitions from the above states.

In addition, the present data allowed the observation of a second isomer at 250 keV lying above the $3^+$ isomer. Figure 4(a) shows a timing curve when making the $\gamma$(start)-$\gamma$(stop) coincidence with the transitions populating and depopulating the 250-keV level. From this $\gamma$-$\gamma$-$t$ data, the half-life was estimated to be 13.4(8) ns. The $4^-$ state at 123 keV also turned out to be an isomer with a half-life of 10.6(3) ns as shown in Fig. 4(b), which is in good agreement with the previous result 9.6(10) ns [14]. We notice that the states of $5^-$ at 275 keV, $6^-$ at 287 keV, and $7^-$ at 311 keV showed no isomeric characteristic in $\gamma$-$\gamma$-$t$ spectra when applying the combination of depopulating and populating transitions such as 152–143 keV and 164–791, 625, 768, 272 keV. Further, the present data suggest another isomer at 689 keV. Figure 4(c) shows the time-difference spectra between the transitions feeding and depopulating of the $8^-$ state at 689 keV (band 6 head), yielding a half-life of 13.7(4) ns. Through lifetime analysis and coincidence relationships, the four $\gamma$-ray transitions with energies 130, 133, 236, and 378 keV decaying from the 689-keV isomer could be placed in the level scheme as shown in Fig. 2. It is worth noting that the identification of the $J^\pi = 8^-$ isomer completes the systematics of the isomeric $8^-$ and/or $7^-$ states in odd-odd I isotopes from $N = 63$, $^{116}$I, to $N = 71$, $^{124}$I, built on the proton-hole $g_{9/2}$ orbital coupled to the neutron $h_{11/2}$ orbital [10]. The isomeric states identified in the present work are denoted in Table I as including their half-lives.

We have identified numerous collective bands, which are labeled from 1 to 9 in Fig. 2. Among them, band 5 was observed as well in Ref. [11]. Figure 5 presents $\gamma$-ray transitions belonging to bands 1 to 6 that were strongly populated. In contrast, bands 7 to 9 were weakly populated as follows: the intensity of the 176-keV transition fed by bands 7 to 9 amounts to 4% relative to the 123 keV transition from bands 1–6. Figure 6 shows $\gamma$-ray peaks assigned to bands 7 to 9 including lower-lying transitions. One can see that the transitions feeding the 55-keV isomer are clearly identified under the early delayed gating condition (150–850 ns). We summarize the experimental results associated with the $\gamma$-ray transitions belonging to $^{124}$I in Table I, where the energies, relative intensities, DCO ratio values, and spin-parity assignments are included.

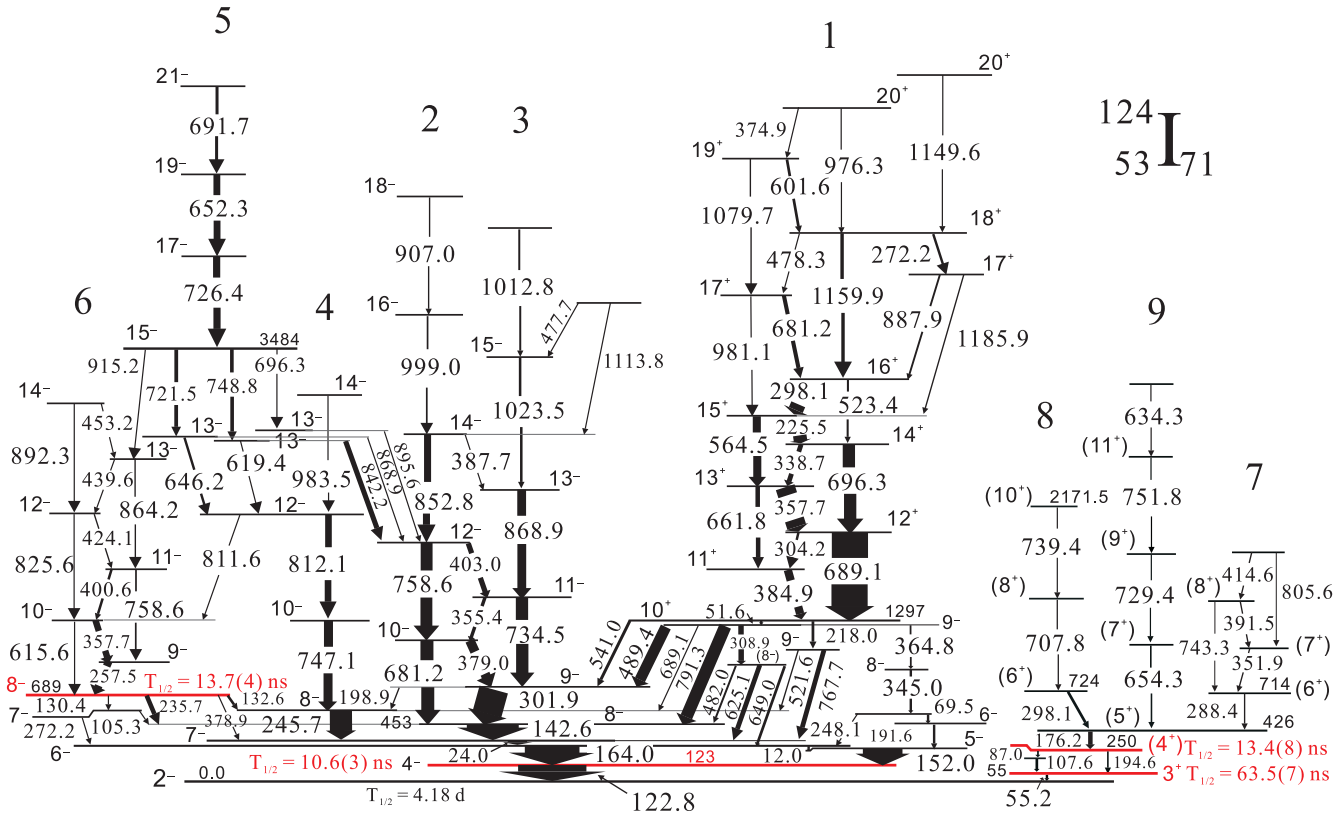


FIG. 2. Level scheme of $^{124}$I deduced from the present work with the $^{122}$Sn($^{7}$Li, 5$n$) $^{124}$I reaction at $E_{\rm lab}$ = 54 MeV. The isomers identified in the present work are indicated in red color and the lifetimes are given in nanoseconds with statistical uncertainties. The energies of the excited states and $\gamma$ rays are given in keV. The widths of the arrows represent relative intensities. The different bands are labeled with large numbers 1–9. The levels with uncertain spin-parity assignments are denoted with brackets.

## IV. DISCUSSION

In the neighboring odd-mass $^{123}$I, the spin-parities are found to be $5/2^+$ ($\pi d_{5/2}$) for the ground state and $7/2^+$ ($\pi g_{7/2}$) for the first excited state at 138 keV. On the other hand, the $11/2^-$ level at 944 keV, where the negative-parity collective bands are well developed, is related to the proton intruder $h_{11/2}$ orbital. In the neighboring odd-neutron $^{123}$Te, the ground and first excited states have $J^\pi = 1/2^+$ and $3/2^+$ that originate from the neutron $s_{1/2}$ and $d_{3/2}$ orbitals, respectively. The $11/2^-$ level based on the neutron $h_{11/2}$ orbital has also been observed at a much lower energy than that of $^{123}$I, at 248 keV. Accordingly, low-lying states in $^{124}$I are expected to be dominantly produced by the following proton-neutron configurations: $\pi d_{5/2}\nu h_{11/2}$ and $\pi g_{7/2}\nu h_{11/2}$ as a negative parity and $\pi(d_{5/2}, g_{7/2})\nu d_{3/2}$, $(d_{5/2}, g_{7/2})\nu s_{1/2}$, and $\pi h_{11/2}\nu h_{11/2}$ as a positive parity. Consequently, the $2^-$ ground state and the negative parity states below $8^-$ are supposed to be members of the multiplet based on the $\pi d_{5/2}$(or $g_{7/2}$)$\nu h_{11/2}$ configurations. In contrast, low-lying positive-parity states below $5^+$ can be interpreted as members of the multiplet due to the $\pi(d_{5/2}, g_{7/2})\nu s_{1/2}$ and $\pi(d_{5/2}, g_{7/2})\nu d_{3/2}$ configurations. The $8^-$ and $9^-$ states on which collective bands are built are most likely to be associated with the $\pi g_{7/2}\nu h_{11/2}$ configuration. In the odd-mass I isotopes, strongly coupled rotational bands were found and interpreted as being attributed to the proton hole $g_{9/2}$ excitation below the proton $Z = 50$ shell gap. The $8^-$ isomer at 689 keV is associated with the proton hole in the $g_{9/2}$ orbital coupled to the neutron $h_{11/2}$ orbital, on which the coupled rotational band, band 6, is built. In this paper, we mainly focus on the collective bands built on the aforementioned low-lying states.

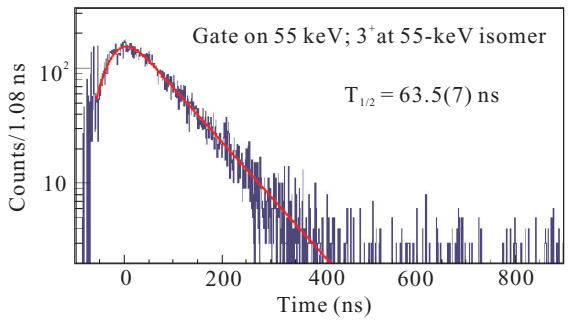


FIG. 3. $\gamma$-ray time spectrum from the beam-$\gamma$ data when gating on the 55-keV transition, including a fit to the data. The fit was made with a convolution function based on the maximum likelihood methods. The number in parentheses is the statistical error in the last digit.

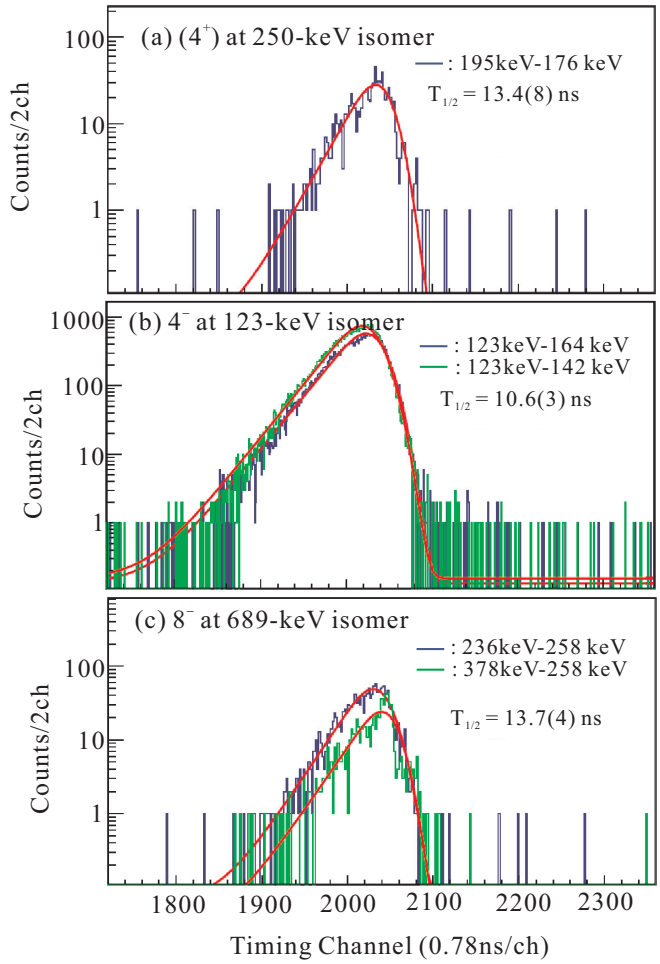


FIG. 4. Decay time curves based on $\gamma$-$\gamma$-$t$ data, including fitted lines for the levels at (a) 250 keV, (b) 123 keV, and (c) 689 keV. The numbers in parentheses are the errors in the last digit.

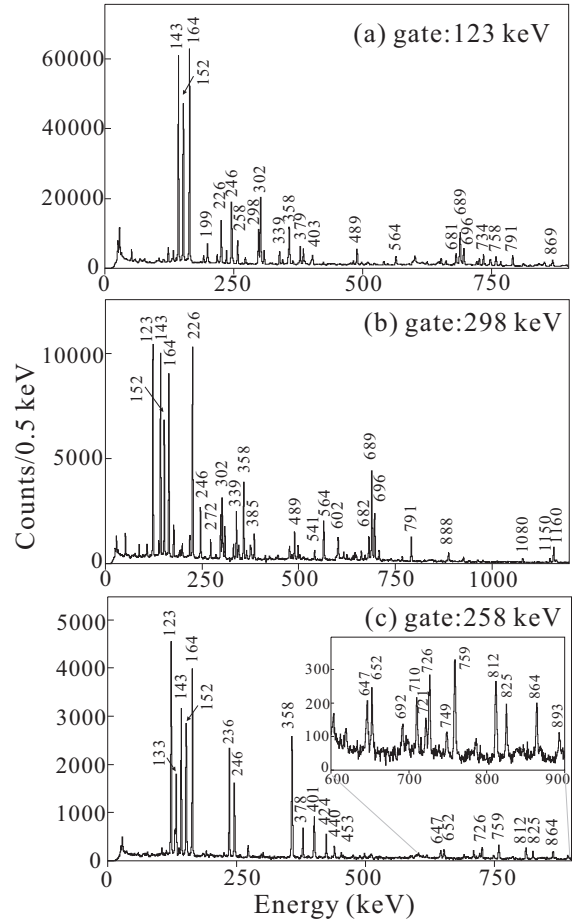


FIG. 5. $\gamma$-ray transitions in the excited states of $^{124}$I populated by the $^{122}$Sn($^{7}$Li, 5$n$) reaction at a beam energy of 54 MeV: (a) $\gamma$ rays in coincidence with the 123-keV transition, (b) rays in coincidence with the 298-keV transition belonging to band 1, and (c) $\gamma$ rays in coincidence with the 258-keV transition belonging to band 6. Energies are in keV.

Band 1 built on the $10^+$ state at 1297 keV was suggested to be associated with the $\pi h_{11/2}\nu h_{11/2}$ configuration [9,15]. In both $^{123}$I and $^{123}$Te, the levels on the $11/2^-$ state consist of the yrast sequence. We notice that the excitation energy of the $10^+$ bandhead is consistent with the sum of excitation energies of the $11/2^-$ levels at 948 keV in $^{123}$I and at 248 keV in $^{123}$Te. This aspect suggests that band 1 should be attributed to the coupling of the proton $h_{11/2}$ orbital to the neutron $h_{11/2}$ orbital. Next, the negative-parity collective bands can be interpreted as originating from the coupling of the proton $g_{7/2}$ (or $d_{5/2}$) orbital to the neutron $h_{11/2}$ orbital.

The plot of excitation energy ($E$) difference versus angular momentum (total spin $J$) gives comprehensive information on nuclear structures according to changes in energy trends. Specifically, the slopes of such lines correlate with various structural phenomena: the constant, monotonically increasing, irregular, and dip values correspond to vibrational, rotational, single-particle, and energetically favored multinucleon alignment modes, respectively. As shown in Fig. 7, the negative-parity bands indicate a deformed rotational structure while band 1 below $15^+$ shows a quadrupole vibrational structure. We find that band 1 has local minima at $15^+$ and $16^+$ while it reveals a single-particle structure at $18^+$ and $20^+$. For bands 2 and 3, the constant values close to 500 keV/$\hbar$ imply two-neutron alignments in the $h_{11/2}$ orbital, which will be discussed later.

To understand shape structures of the observed collective bands, we have carried out self-consistent deformation calculations for proton-neutron quasiparticle configurations based on the total Routhian surface (TRS) formalism [16,17]. These calculations are based on a universal Woods-Saxon single-particle potential and a monopole pairing residual interaction, where the pairing gaps have been calculated at zero frequency and allowed to decrease with increasing rotational frequency. Figure 8 presents TRS plots in the polar coordinate plane $(\beta_2, \gamma)$ for the favored and unfavored states of the $\pi h_{11/2}\nu h_{11/2}$ configuration. Here, the favored and unfavored states correspond to the odd-spin and even-spin members according to the definition of parity and signature components. As shown in Fig. 8, the TRS calculations predict a shallow minimum with a noncollective oblate shape. This result

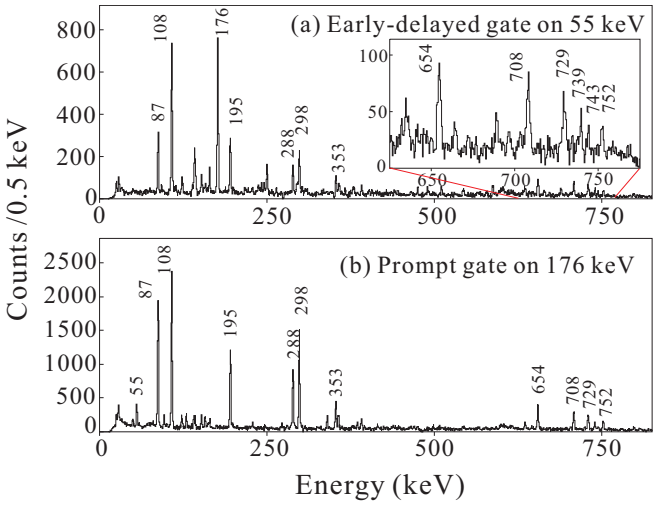


FIG. 6. (a) Early delayed (150–850 ns) coincidence $\gamma$-ray spectrum by gating on the 55-keV transition depopulating the $3^+$ isomer with a half-life of 63.5(7) ns. (b) Prompt coincidence ($\pm$140 ns) $\gamma$-ray spectrum by gating on the 176-keV transition fed by bands 7 to 9.

supports the emergence of a quadrupole vibrational structure for this configuration.

Figure 9 shows the excited states built on the $\pi h_{11/2}\nu h_{11/2}$ configuration in $^{124}$I and those built on the $\nu h_{11/2}$ orbital in $^{123}$Te [18]. From this comparison, we find a similar structure between the cascade of transitions connecting the $20^+$ state to the $10^+$ state in $^{124}$I with the cascade between the $31/2^-$ state and the $11/2^-$ state in $^{123}$Te. An additional feature worth noticing is that the $16^+$ and $15^+$ states of $^{124}$I and the $23/2^-$ and $21/2^-$ states of $^{123}$Te are positioned at relatively low energies. These energetically favored states are interpreted as being due to a full alignment of a pair of protons in the $g_{7/2}$ orbital outside $Z = 50$, leading to the $6^+$ state in Te isotopes. Given the four nucleons in a $\pi(g_{7/2})^2 h_{11/2}\nu h_{11/2}$ configuration, the TRS calculations reproduce the energetically favored states at $15^+$ and at $16^+$, respectively, as indicating a noncollective oblate shape with $\beta_2 = 0.16$ and $\gamma = 60°$. As shown

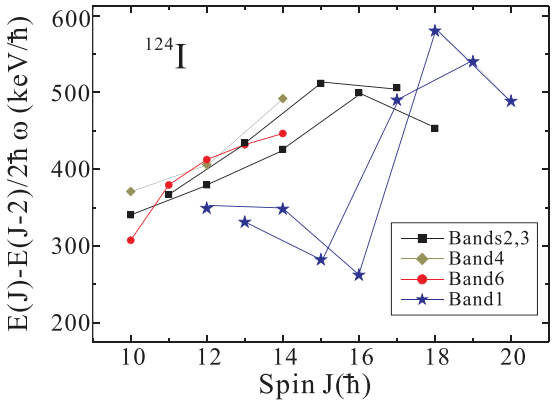


FIG. 7. Plot of angular frequency (keV/$\hbar$) versus angular momentum $J$ (spin $\hbar$) for the bands in $^{124}$I.

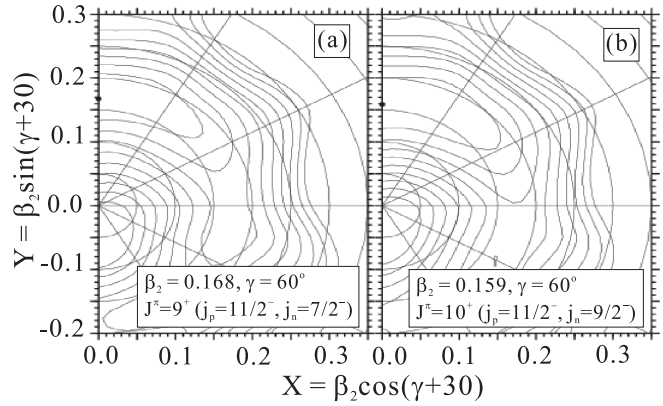


FIG. 8. Plots of total Routhian surface calculations at $\hbar\omega = 0.18$ MeV for (a) the favored (odd spin) and (b) unfavored (even spin) states for the $\pi h_{11/2}\nu h_{11/2}$ configuration.

in Fig. 10, the spins of $15^+$ and $16^+$ are generated by $j_p = 23/2$ coupled to $j_n = 7/2$ and $j_n = 9/2$, respectively. Consequently, the $16^+$ and $15^+$ states are also built on the two-proton alignment of $6^+$ in the $g_{7/2}$ orbital coupled to the $10^+$ and $9^+$ states due to the $\pi h_{11/2}\nu h_{11/2}$ alignment, respectively. Moreover, the total Routhian surfaces show another minimum at $21^-$ when coupling this four-quasiparticle configuration to two neutrons in the $h_{11/2}$ orbital, $\pi(g_{7/2})^2(h_{11/2})\nu h_{11/2})^3$. However, the corresponding noncollective state could not be observed in the present experiment even though they were found at $33/2^-$ and $35/2^-$ in $^{123}$Te. It is worth noticing that in $^{120}$I a six-nucleon noncollective isomer was observed at $j^\pi = 25^+$ [19]. This is the case of full alignment of six valence nucleons outside the $^{114}$Sn core, $Z = 50$ and $N = 64$: three protons $(g_{7/2})^1(d_{5/2})^1(h_{11/2})^1$ and three neutrons $(h_{11/2})^3$.

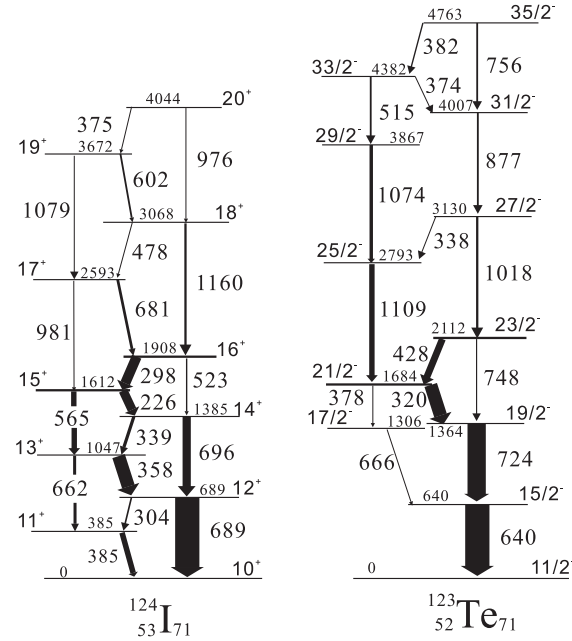


FIG. 9. Comparison between the states based on the $\pi h_{11/2}\nu h_{11/2}$ orbital in $^{124}$I and the $\nu h_{11/2}$ orbital in $^{123}$Te [18].

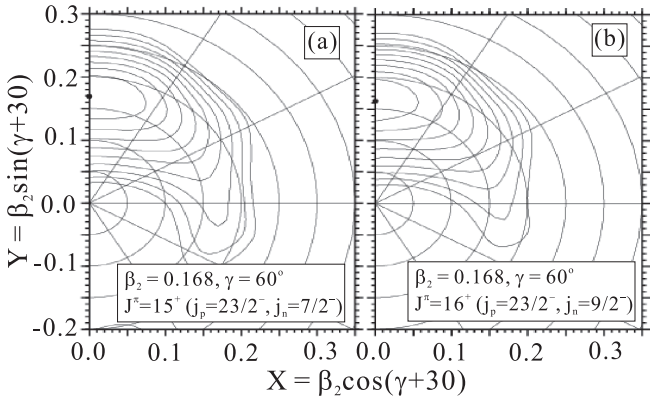


FIG. 10. Plots of total Routhian surface calculations at $\hbar\omega =$ 0.24 MeV for (a) the $15^+$ and (b) the $16^+$ states for the $\pi(g_{7/2})^2(h_{11/2})\nu h_{11/2}$ configuration.

By observing a similar structure between bands 2 and 3, and the collective bands built on the $7/2^+$ state in $^{123}$I, bands 2 and 3 can be understood as being associated with the favored and unfavored signatures of the $\pi g_{7/2}$ orbital coupled to the favored $h_{11/2}$ orbital. According to total Routhian surface calculations for the $\pi g_{7/2}\nu h_{11/2}$ configuration as shown in Fig. 11, energy minima meet at a triaxial shape with $\beta_2 \approx 0.16$ and $\gamma \approx -35^\circ$ over rotational frequencies of 0.18 to 0.3 MeV/$\hbar$. Thus, the rotational structure of bands 2 and 3 is attributed to the triaxial, collective oblate shape with $\gamma \approx -40^\circ$. In contrast, band 4 can be explained in terms of the unfavored $\nu h_{11/2}$ orbital coupled to the favored $\pi g_{7/2}$ orbital. The TRS calculations for this configuration represent a broad $\gamma$-soft shape toward $\gamma = 60^\circ$ showing a minimum at $+ 50^\circ$. This result suggests that band 4 has a rather vibrational structure. However, band 4 cannot be excluded as being associated with the $\pi d_{5/2}$ orbital coupled to the favored $\nu h_{11/2}$ orbital. Higher-lying transitions above the $13^-$ state can be produced by the second $h_{11/2}$ neutron alignments. The TRS calculations for the $\pi g_{7/2}\nu(h_{11/2})^3$ configuration indicate that surfaces are very soft over $J^\pi = 16^-$ to $17^-$ such that energy minima

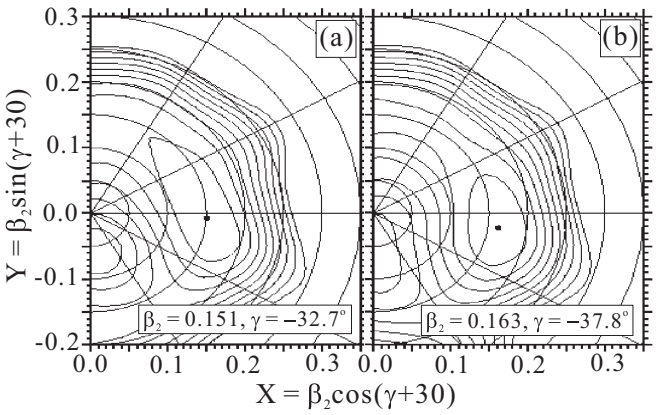


FIG. 11. Plots of total Routhian surface calculations at $\hbar\omega =$ 0.30 MeV for (a) the favored (band 2) and (b) the unfavored (band 3) states based on the $\pi g_{7/2}\nu h_{11/2}$ configuration.

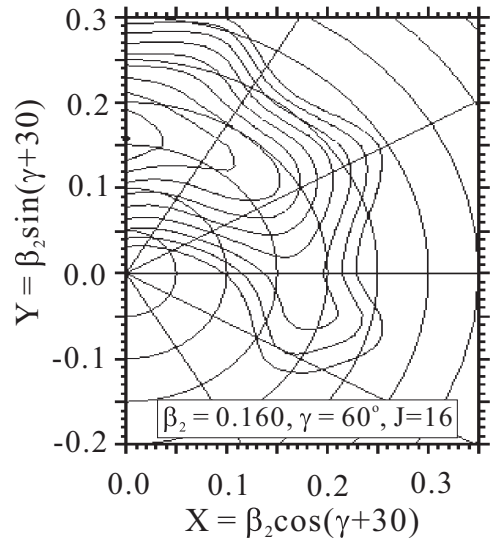


FIG. 12. A plot of total Routhian surface calculations for the $\pi g_{7/2}(h_{11/2})^2\nu h_{11/2}$ configuration at $\hbar\omega = 0.30$ MeV.

move from $\gamma = -50^\circ$ to $+60^\circ$ with increasing frequencies. The very $\gamma$-soft structure explains why the deformed states at higher energies and spins could not be developed.

Band 5 built on the $15^-$ state at 3484 keV shows some peculiar features. First, the decay out of the bandhead is fragmented into the $\pi g_{7/2}\nu h_{11/2}$ states as well as the $\pi g_{9/2}\nu h_{11/2}$ states (band 6) through several transitions. Second, the transition energies indicate a vibrational structure that is somewhat different from the low-lying states. Considering the high excitation energy, this band is most likely a four-quasiparticle excitation. Available negative-parity configurations are the $\pi g_{7/2}(h_{11/2})^2\nu h_{11/2}$ and the $\pi h_{11/2}\nu d_{3/2}(h_{11/2})^2$ configurations. The latter configuration is based on the $\pi h_{11/2}\nu d_{3/2}$ excitation coupled to two neutrons in the $h_{11/2}$ orbital. However, no $\pi h_{11/2}\nu d_{3/2}$ band was observed. Besides, the TRS calculations indicate that this $\pi h_{11/2}\nu d_{3/2}$ configuration tends to produce a triaxial collective shape with $\beta_2 \approx 0.18$ and $\gamma \approx +30^\circ$. Therefore, we conclude that band 5 may not be related to the $\pi h_{11/2}\nu d_{3/2}(h_{11/2})^2$ configuration. Instead, this band is likely to be associated with the $\pi g_{7/2}(h_{11/2})^2\nu h_{11/2}$ structure based on the $\pi g_{7/2}\nu h_{11/2}$ orbital (bands 2 and 3) coupled to two protons in the $h_{11/2}$ orbital. As Fig. 12 shows, this $\pi g_{7/2}(h_{11/2})^2\nu h_{11/2}$ configuration is believed to be a non-collective oblate shape showing energy minima at $16^-$ and $17^-$. Many transitions out of the $15^-$ state to the $\pi g_{7/2}\nu h_{11/2}$ states are considered to be due to a large shape difference between band 5 and band 2 (or 3).

As already mentioned, band 6 can be explained in terms of a proton-hole in the $g_{9/2}$ orbital coupled to a neutron in the $h_{11/2}$ orbital, the $\pi g_{9/2}\nu h_{11/2}$ configuration. In the region of nuclei around the $Z = 50$ shell gap, both the $g_{9/2}$ and $h_{11/2}$ intruder subshells are present near Fermi surfaces. If both the unpaired proton and neutron occupy high-$\Omega$ orbitals of these intruder subshells, high-$K$ states can occur at low excitation energies and then result in hindered decays to low-$K$ states ($K$ trap isomerism) [6,7]. These $K$

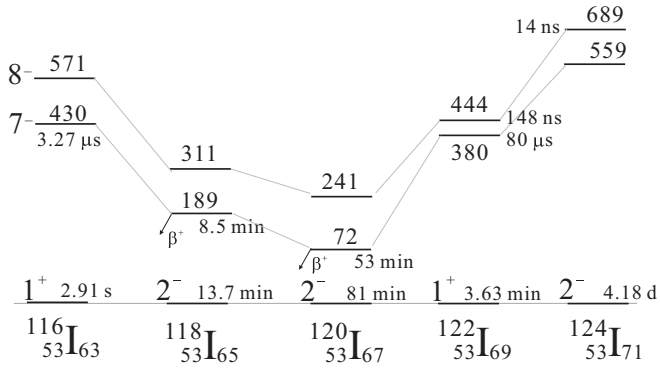


FIG. 13. Systematics of energies and half-lives for the excited states of $8^-$ and $7^-$ based on the $\pi g_{9/2}\nu h_{11/2}$ configuration in $^{116}$I [20], $^{118}$I [21], $^{120}$I [22], $^{122}$I [13] and $^{124}$I in the present work. The energies are given in keV.

isomers are systematically observed firstly at $J^\pi = 7^-$ that originates from $K^\pi = \Omega_p(= 9/2) + \Omega_n(= 5/2) = 7^-$ states based on the proton-neutron $\pi g_{9/2}[404]9/2\ \nu h_{11/2}[532]5/2$ configuration for $^{116}$I up to $^{122}$I, and at $J^\pi = 8^-$ based on the $\pi g_{9/2}[404]9/2\ \nu h_{11/2}[523]7/2$ configuration for $^{122}$I and $^{124}$I. Figure 13 shows the level systematics for these high-K isomers from $^{116}$I to $^{124}$I. We observe two distinctive features in this figure. First, there is a concave trend with a minimum energy around $N = 66$, which corresponds to the center of the major shell between $N = 50$ and 82. It is worth noting that a half-occupancy in a main shell or a subshell drives a nucleus to a large deformation. See also Fig. 1(a) for this effect. Second, the $K$ isomers move from $7^-$ to $8^-$ with increasing neutrons. Of course, this transition comes from the change of a Nilsson configuration of [532]5/2 to [523]7/2 in the neutron $h_{11/2}$ orbital.

Band 7 built on the $6^+$ state at 715 keV also shows a typical coupled rotational structure. As neutron number increases, it is found that the $\nu d_{3/2}$ orbital in the odd-mass Te is favored in energy, and becomes the ground level configuration. Hence, the $6^+$ state and the emerging collective structure can be understood as being associated with the proton-hole $g_{9/2}$ orbital coupled to the neutron $d_{3/2}$ orbital. In contrast, bands 8 and 9 showing a weak quadrupole rotational structure might be associated with the $\pi g_{7/2}\nu d_{3/2}$ configuration. Ssimilar bands have been observed in the neighboring $^{122}$I [13] and $^{126}$I [8].

## V. CONCLUSIONS

The excited states of $^{124}$I have been investigated using the fusion-evaporation reaction of $^{122}$Sn($^7$Li, $5n$)$^{124}$I with a beam energy of 54 MeV. Through in-beam and out-of-beam $\gamma$-ray spectroscopy, we have identified numerous low-lying, noncollective proton-neutron coupled states including isomers and collective states. Among them, a positive-parity band above $J^\pi = 10^+$ was interpreted as being associated with the $\pi h_{11/2}\nu h_{11/2}$ configuration. This band follows a Te core structure showing a typical quadrupole vibration. In contrast, the negative parity bands based on the $\pi g_{7/2}\nu h_{11/2}$ configuration exhibit a soft triaxial deformed rotation. A proton-hole excitation in the $g_{9/2}$ orbital below the $Z = 50$ shell gap gives rise to two coupled rotational bands; one is built on the $8^-$ isomeric state with a half-life of 13.7(4) ns when coupling to the neutron $h_{11/2}$ orbital, and another is built on the $6^+$ state when coupling to the neutron $d_{3/2}$ orbital. The observation of the isomer at $J^\pi = 8^-$ completes the systematic features of high-$K$ isomers due to the $\pi g_{9/2}\nu h_{11/2}$ configuration in $^{116}$I ($N = 63$) up to $^{124}$I ($N = 71$).

## ACKNOWLEDGMENTS

This work was supported by the Institute for Basic Science, Korea under project code IBS-R031-D1.

[1] K. Heyde and J. L. Wood, Rev. Mod. Phys. **83**, 1467 (2011).
[2] J. H. Hamilton, in *Treatise Heavy Ion Science, Volume 8: Nuclei Far From Stability*, edited by D. A. Bromly (Plenum, New York and London, 1980), pp. 3–98.
[3] K. Heyde, P. van Isacker, M. Waroquier, J. L. Wood, and R. A. Meyer, Phys. Rep. **102**, 291 (1983).
[4] J. L. Wood, K. Heyde, W. Nazarewicz, M. Huyse, and P. van Duppen, Phys. Rep. **215**, 101 (1992).
[5] National Nuclear Data Center (NNDC), http://www.nndc.bnl.gov/chart/
[6] P. Walker and G. Dracoulis, Nature (London) **399**, 35 (1999).
[7] G. D. Dracoulis, Phys. Scr. T **88**, 54 (2000).
[8] C.-B. Moon, G. D. Dracoulis, R. A. Bark, A. P. Byrne, P. A. Davidson, A. N. Wilson, T. Kibédi, and G. J. Lane, *Department of Nuclear Physics Annual Report 2002*, ANU-P/1564 (The Australian National University, Canberra, 2002), pp. 11–17.
[9] C.-B. Moon, G. D. Dracoulis, R. A. Bark, A. P. Byrne, P. A. Davidson, A. N. Wilson, A. M. Baxter, T. Kibédi, and G. J. Lane, J. Korean Phys. Soc. **43**, S100 (2003).
[10] C.-B. Moon, G. D. Dracoulis, R. A. Bark, A. P. Byrne, P. A. Davidson, T. Kibédi, G. J. Lane, and A. N. Wilson, J. Korean Phys. Soc. **59**, 1525 (2011).
[11] D. L. Balabanski, G. Rainovski, N. Blasi, G. Lo Bianco, G. Falconi, S. Signorelli, D. Bazzacco, G. de Angelis, D. R. Napoli, A. A. Cardona, A. J. Krainer, and H. Somacal, Acta Phys. N. S. **6**, 275 (1997).
[12] https://physics.anu.edu.au/nuclear/hiaf.php
[13] B. Moon, C.-B. Moon, G. D. Dracoulis, R. A. Bark, A. P. Byrne, P. A. Davidson, G. J. Lane, T. Kibédi, A. N. Wilson, and C. Yuan, Phys. Rev. C **100**, 024319 (2019).
[14] J. Burde, V. Richter, J. Tsaliah, and I. Labaton, Nucl. Phys. A **385**, 29 (1982).
[15] C.-B. Moon, J. Korean Phys. Soc. **44**, 244 (2004).
[16] R. Wyss, J. Nyberg, A. Johnson, T. Bengtsson, and W. Nazarewicz, Phys. Lett. B **215**, 211 (1988).
[17] W. Nazarewicz, R. Wyss, and A. Johnson, Nucl. Phys. A **503**, 285 (1989).

[18] N. Blasi, G. Lo Bianco, Ch. Protochristov, D. Bazzacco, G. Falconi, N. H. Medina, G. De Angelis, and D. R. Napoli, Z. Phys. A **354**, 233 (1996).

[19] B. Moon, C.-B. Moon, G. D. Dracoulis, R. A. Bark, A. P. Byrne, P. A. Davidson, G. J. Lane, T. Kibédi, A. N. Wilson, C. Yuan, and B. Hong, Phys. Lett. B **782**, 602 (2018).

[20] C.-B. Moon, T. Komatsubara, and K. Furuno, Nucl. Phys. A **730**, 3 (2004).

[21] C.-B. Moon, T. Komatsubara, T. Shizuma, Y. Sasaki, K. Furuno, and C. S. Lee, Nucl. Phys. A **728**, 350 (2003).

[22] L. Li, J. Sun, J. Li, D. Yu, G. Liu, W. Zhang, K. Ma, D. Yang, Y. Ma, X. Wu, L. Zhu, C. He, Y. Zheng, S. Yao, C. Li, S. Hu, X. Cao, J. wang, and B. Yu, Chin. Phys. Lett. **30**, 062301 (2013).